

SIMULATIONS OF MAGNETOHYDRODYNAMICS AND CO FORMATION FROM THE CONVECTION ZONE TO THE CHROMOSPHERE

Sven Wedemeyer-Böhm¹, Werner Schaffenberger¹, Oskar Steiner¹, Matthias Steffen², Bernd Freytag³, and Inga Kamp⁴

¹Kiepenheuer-Institut für Sonnenphysik, Schöneckstr. 6, 79104 Freiburg, Germany

²Astrophysikalisches Institut Potsdam, An der Sternwarte 16, 14482 Potsdam, Germany

³Los Alamos National Laboratory/Depart. of Phys. and Astron. at Michigan State University, USA

⁴Space Telescope Division of ESA, STScI, Baltimore, USA

ABSTRACT

We present the results of simulations of the formation and the evolution of carbon monoxide (CO) and of magnetic fields in the solar atmosphere, extending from the upper convection zone to the middle chromosphere. The radiation hydrodynamics code CO⁵BOLD has been extended to a magnetohydrodynamics version. Furthermore, the time-dependent treatment of chemical reaction networks has been added. Next to the time-dependent solution of the reaction network, the code accounts for the advection of the resulting particle number densities with the hydrodynamic flow field and also for the radiative cooling by carbon monoxide lines.

Although the largest absolute amount of CO is located in the middle photosphere, CO is also abundant in the layers above and binds a large fraction of carbon. An exception are the hot propagating shock waves that frequently dissociate the carbon monoxide molecules.

These shock waves, which are a ubiquitous phenomenon in the model chromosphere, also shape the magnetic field of these layers. As a result the chromosphere is characterised by highly dynamic magnetic filaments that are formed in the compression zone behind and along shocks. Nevertheless, the magnetic field in the chromosphere is much more homogeneous than in the photosphere below, resulting in a dynamic small-scale 'canopy' at the boundary of these layers.

Key words: Sun, chromosphere, chemistry, magnetic fields.

1. INTRODUCTION

Despite much progress during the last years, many questions concerning the chromosphere of the Sun remain open. A self-consistent and comprehensive three-dimensional time-dependent numerical model, matching all accessible chromospheric diagnostics, is of essential importance to gain insight in the dynamic and inhomogeneous structure of the solar chromosphere. Unfortunately, modelling the chromosphere is a numerically very demanding task since a realistic description of this layer requires the inclusion of many physical ingredients. In order to make progress, the radiation magnetohydrodynamics code CO⁵BOLD (Freytag et al., 2002) has been upgraded recently. It now offers a large range of possible applications. For instance, it is used for 2D and 3D simulations of the formation and destruction of carbon monoxide (CO) in the non-magnetic solar photosphere and low chromosphere, including radiative cooling due to spectral lines of CO that was considered being an important cooling agent for long time. First 2D and 3D simulations with the new magnetohydrodynamics (MHD) version are currently in progress.

Here we focus on a recently calculated MHD model with carbon monoxide chemistry and radiative cooling that extends from the upper convection zone to the low/middle chromosphere.

2. THE CODE

The numerical simulations presented here were all carried out with the code CO⁵BOLD (Freytag et al., 2002; Wedemeyer et al., 2004). It is designed for simulating hydrodynamics and radiative transfer in the convective layers of stars and offers a range of

additional features, e.g. the treatment of dust formation in stellar atmospheres (Höfner et al., 2004). Recently, the code has been extended to treat magnetohydrodynamics (see Schaffenberger et al. in these proceedings). Moreover, the time-dependent treatment of chemical reaction networks has been implemented. The changes of the number densities of chemical species due to chemical reactions, the advection with the hydrodynamic flow field, and even radiative cooling due to spectral lines of carbon monoxide are taken into account (Wedemeyer-Böhm et al., 2005; Wedemeyer-Böhm & Steffen, in prep.). Time-dependent hydrogen ionisation is the latest new option, although hydrogen is treated as a minority species only so far (Leenaarts & Wedemeyer-Böhm, in prep.).

In CO⁵BOLD operator splitting allows to treat hydrodynamics, tensor viscosity, chemistry, and radiative transfer in subsequent steps of this order. The overall computational time step is typically around 0.1 s to 0.2 s for non-magnetic simulations but up to a factor ten smaller for the MHD case, depending on magnetic field strength. A second order accurate HLL-solver was chosen for the extension to magnetohydrodynamics. For more details of the numerical scheme see the contribution by Schaffenberger et al. (in these proceedings). The advantage of the new MHD code is that its special design, using an approximate Riemann-type solver, allows the simulation of magnetic fields in the solar chromosphere where the frequent formation of shocks causes traditional finite difference schemes to fail.

The advection of chemical species and the solution of the system of chemical reactions are separated. The advection with the hydrodynamic flow field is done analogously to the gas density within the HD/MHD solver. The chemical evolution is then calculated for each grid cell separately and starts with the computation of the reaction rates. The rates depend on the local temperature and the number densities of the chemical species. The solution of the resulting system of first order differential equations then yields the number densities at the new time.

For the radiative cooling due to carbon monoxide spectral lines an additional opacity band in the infrared wavelength range has been introduced (Wedemeyer-Böhm & Steffen, in prep.). It accounts for the opacity around a wavelength of $\lambda = 4.7 \mu\text{m}$ where the fundamental vibration rotation lines of carbon monoxide are located. The additional CO opacity is calculated from the time-dependent CO number density using approximate opacity distribution functions (ODFs). The radiation transport is then solved in a Rosseland mean opacity band and the IR band and results in a net radiative heating rate that is finally used to update the internal energy of the gas.

The lateral boundary conditions are periodic whereas

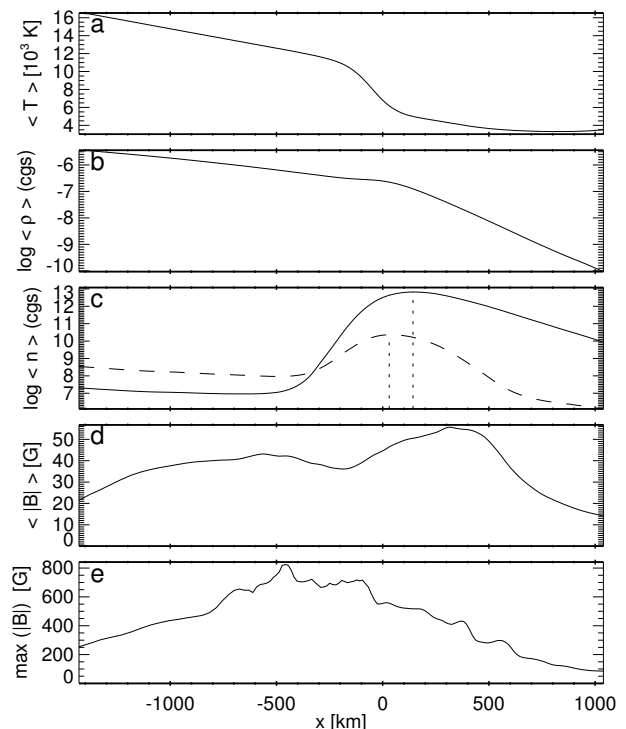


Figure 1. Average stratification of the 2D MHD model with CO chemistry and radiative cooling. **a)** gas temperature T , **b)** logarithmic gas density ρ , **c)** logarithmic number densities of CO (n_{CO} , solid) and CH (n_{CH} , dashed), and **d)** absolute magnetic field $|B|$. Panel **e)** shows the maximum magnetic field strength. The vertical dotted lines in panel **c)** mark the maxima of the average distributions.

the lower boundary is “open”, i.e. material can flow in and out of the computational box. The upper boundary condition is usually of ‘transmitting’ type in our non-magnetic simulations so that shock waves can leave the computational domain without being reflected. Examples are the simulations of the dynamics of the solar chromosphere (Wedemeyer et al., 2004) and of the formation of carbon monoxide in the solar atmosphere (Wedemeyer-Böhm et al., 2005). In the MHD case, however, the upper boundary can only be treated as closed so far.

3. THE MODELS

The 2D model with magnetic fields, chemical reaction network for CO, and its radiative cooling extends 4800 km in horizontal and 2500 km in vertical direction. The origin of the height axis is adjusted to the average level of optical depth unity. The lower boundary is therefore located at -1450 km and the upper at 1050 km. The initial model was extracted from a non-magnetic 2D simulation (Wedemeyer, 2003). A homogeneous vertical magnetic field of a flux density of 10 G, corresponding to fields in

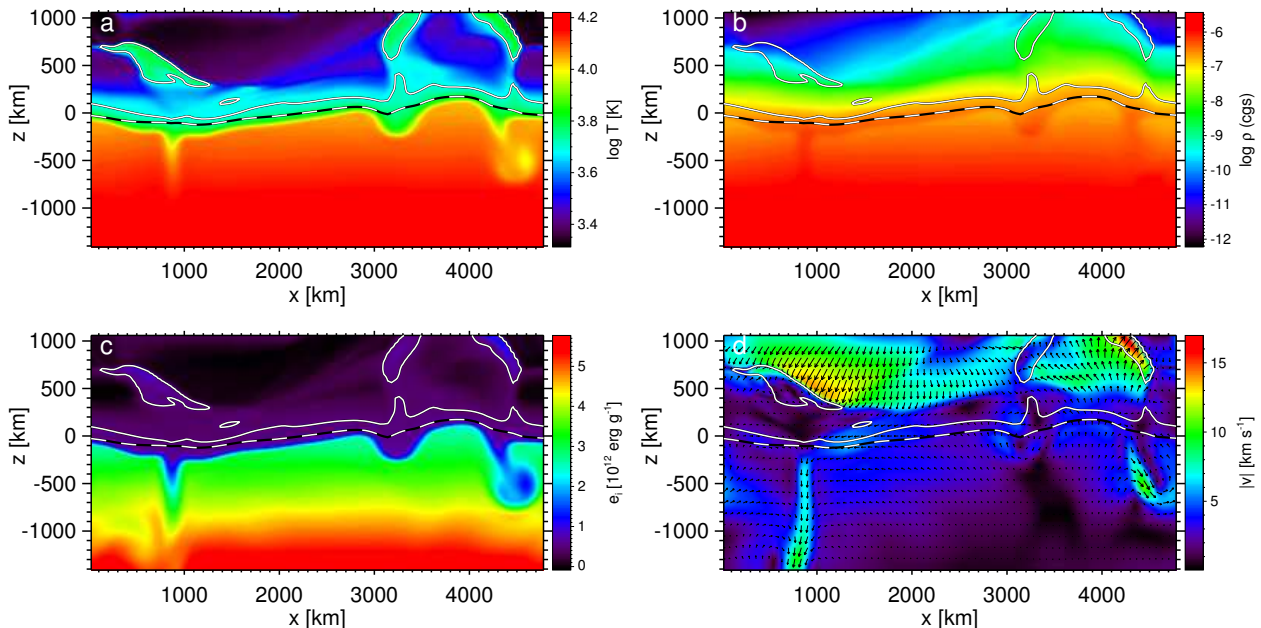


Figure 2. Exemplary snapshot from the 2D MHD simulation including chemistry: **a)** logarithmic gas temperature T , **b)** logarithmic gas density ρ , **c)** internal energy e_i , and **d)** absolute velocity $|v|$ with arrows indicating the flow direction (\vec{v}). The height of optical depth unity is drawn as dashed line. The solid line is a contour for a gas temperature of $T = 5000$ K.

network-cell interiors, and number density arrays for the chemical species were added. A total duration of 9600s is available for this simulation with the first 3600s excluded from analysis to ensure relaxation of the model. An additional simulation run with a higher initial field of $B_0 = 100$ G is currently in progress.

The resulting stratification of the model with $B_0 = 10$ G, averaged horizontally and in time, is shown for various quantities in Fig. 1, whereas Figs. 2-4 display an exemplary snapshot from the simulation. The quantities in Fig. 2 reveal the structural differences of the included layers. The top of the convection zone is characterised by comparably large spatial scales and long dynamical timescales. The bottom of the photosphere features granule interiors with upward flowing hot gas and cool narrow downdrafts that form intergranular lanes when seen from above. In contrast, the upper layer of the model, the chromosphere, is made up of a cool background and ubiquitous hot propagating shock waves that evolve on very short timescales.

We also have a first 3D MHD model with 120^3 cells and an extension of $4780 \times 4780 \times 2790$ km. The initial model was extracted from a previously computed, relaxed non-magnetic model, too. Again, a homogeneous vertical magnetic field of a flux density of 10 G was superposed. So far a full hour simulation time is available. This model is described in more detail by Schaffenberger et al. in these proceedings.

4. CHEMISTRY

4.1. Chemical reaction network

The chemical reaction network used here takes into account the reactions that are most important for the formation and dissociation of CO under the physical conditions of the solar atmosphere. The network connects the chemical species H, H_2 , C, O, CO, CH, OH, and a representative metal, by 27 reactions (for details see Wedemeyer-Böhm et al., 2005).

The abundance of helium was adopted for the “representative metal”, which acts as catalytic element, thus providing a upper limit for the influence of the “metal”. Photoreactions and ion-molecule reactions are excluded because they have only negligible influence on the total CO concentration for heights ≤ 1000 km in the solar atmosphere (Asensio Ramos et al., 2003).

We exclude nitrogen chemistry in our reaction network since tests showed that it is negligible for the formation of carbon monoxide in the solar atmosphere (Wedemeyer-Böhm et al., 2005).

Simulations with altered reaction networks, excluding particular species and/or reactions or even whole branches, reveal that the most important formation channel for carbon monoxide in the solar atmosphere is the one via hydroxide (OH).

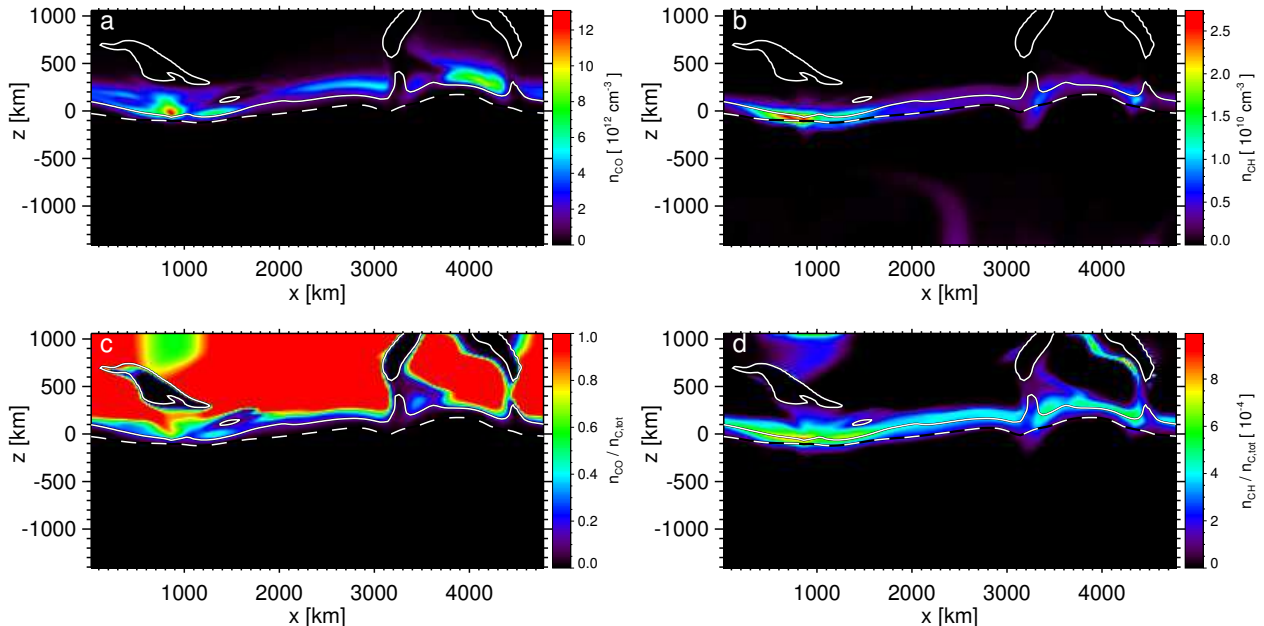


Figure 3. Same snapshot as in Fig. 2. **a)** CO number density n_{CO} , **b)** CH number density n_{CH} , **c)** fraction of C atoms bound in CO ($n_{\text{CO}}/n_{\text{C,tot}}$), and **d)** fraction of C atoms bound in CH ($n_{\text{CH}}/n_{\text{C,tot}}$). The height of optical depth unity is drawn as dashed line. The solid line is a contour for a gas temperature of $T = 5000$ K.

4.2. Carbon monoxide

The resulting number density of carbon monoxide (Fig. 3a) is similar to the results of earlier non-magnetic simulations (Wedemeyer-Böhmer et al., 2005). The highest absolute density of CO is located in the cool regions in the middle photosphere, mapping the reversed granulation pattern. The low temperatures in these regions lead to a strong and almost instantaneous formation of carbon monoxide. The warm regions, caused by compression during the deflection of lateral flows into the downdrafts, are void of CO. The same is true for the hot propagating shock waves in the chromosphere above. Although the bulk of CO is found in the middle photosphere, peaking at $z \sim 140$ km (Fig. 1), a result that is line with earlier findings by Uitenbroek (2000) and Asensio Ramos et al. (2003), its relative abundance remains high in the upper layers. This can be seen from the fraction of all carbon atoms ($n_{\text{C,tot}}$) that are bound in CO (Fig. 3c), where the total number density of carbon is defined as

$$n_{\text{C,tot}} = n_{\text{C,atom}} + n_{\text{CO}} + n_{\text{CH}} \quad (1)$$

for the chemical reaction network used here (see Sect. 4.1). While the fraction is zero in the convection zone and in hot atmospheric regions, it can reach even a value of one in a large part of the upper layers, indicating that all available carbon atoms are bound in carbon monoxide molecules.

The assumption of instantaneous chemical equilib-

rium is valid almost everywhere in the model atmosphere but it fails in the vicinity of chromospheric shock waves where the dynamic timescales are shorter than the chemical ones. There, a time-dependent approach is mandatory.

4.3. Carbon monoxide radiative cooling

The influence of the implemented radiative cooling due to CO infrared lines has been analysed by means of 2D simulations with and without the additional cooling. Although there is strong CO cooling in the fronts of propagating shock waves in the chromosphere, the resulting average temperature stratification is only ~ 100 K cooler. That can be explained with the short dynamical timescales that are much shorter than the effective radiative cooling timescale. The time between two successive shock wave heating events is too short for a gas element in the solar atmosphere to relax to a cool state due to carbon monoxide line cooling.

4.4. Methylidyne

Since the chemical reaction network for carbon monoxide includes the methylidyne radical CH, the simulation provides the time-dependent CH number density for all spatial positions and times (Fig. 3b). Obviously the bulk of CH is present in the low pho-

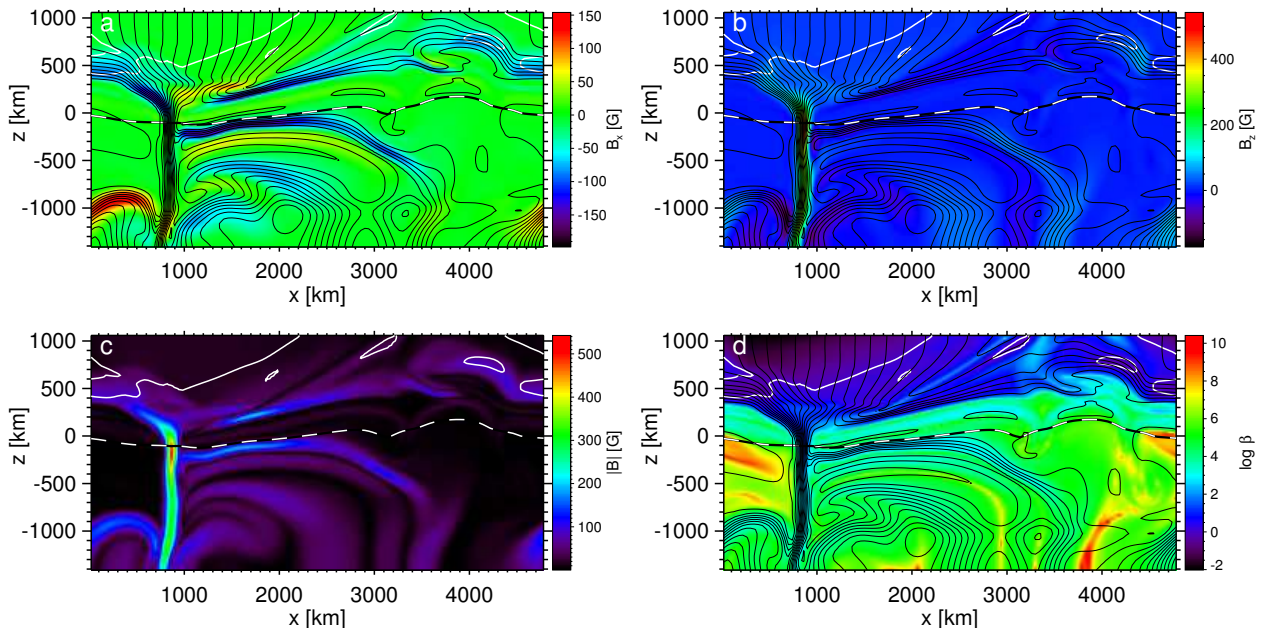


Figure 4. Exemplary snapshot from 2D MHD simulation including chemistry: **a)** horizontal magnetic field component B_x , **b)** vertical magnetic field component B_z , **c)** absolute magnetic field $|B|$, and **d)** logarithmic plasma β . The height of optical depth unity is drawn as dashed line, whereas the solid white contour marks the height of plasma beta $\beta = 1$. The black lines are magnetic field lines.

tosphere close to optical depth unity. It is thus on average located somewhat lower in the atmosphere than CO (Fig. 1), peaking at $z = 30$ km.

But in contrast to CO, methylidyne has no high relative abundance in the upper layers as can be seen from the fraction of all carbon atoms that are bound in CH (Fig. 3d). The fraction hardly reaches a value of 10^{-3} and that only in regions where CO has no significant abundance. Consequently, CH exists in a relatively thin layer in the low photosphere only whereas the more aggressive formation of carbon monoxide let this species dominate almost everywhere above the low photosphere with exception of hot shock waves.

The CH molecule is of particular interest because its spectral lines dominate the so-called ‘‘G band’’ near $\lambda = 430$ nm. Depletion of CH causes its absorption lines to become weaker, resulting in a higher brightness of the G band. This effect is seen in connection with magnetic flux concentrations in the low photosphere that are radiatively heated (see, e.g., Steiner et al., 2001; Schüssler et al., 2003). The resulting increase in gas temperature causes dissociation of CH and thus a lower CH abundance and consequently higher G band brightness at these locations. A preliminary analysis reveals a correlation between magnetic field strength and CH number density similar to the finding by Shelyag et al. (2004).

5. MAGNETIC FIELDS

The horizontal and the vertical components B_x and B_z , as well as the absolute magnetic field $|B|$ are shown in Fig. 4 for the exemplary snapshot. The vertical flux tube at $x = 850$ km has only a weak magnetic field of 540 G. The maximum field strength of the whole sequence is 830 G but only 560 G near optical depth unity (see Fig. 1e). Consequently, no dip in the height of optical depth unity (‘‘Wilson depression’’) and with it no ‘‘hot walls’’ are present that would heat the flux sheet atmosphere. The gas in the weak flux tube in Fig. 4 is even cooler than the ambient medium as can be seen from Fig. 2a, resulting in prominent formation of CO and CH at that location (Fig. 3). This indicates that this weak magnetic structure might even have a negative contrast in the G band. The situation is different for the simulation run with the higher initial field of $B_0 = 100$ G (Fig. 5) with flux tubes of $|B| > 1$ kG. There, a ‘‘Wilson depression’’ and a depletion of CH molecules is seen at the positions of the stronger flux tubes.

In both simulations the flux tubes stay bundled throughout the convection zone down to the lower boundary but spread out with height in the photosphere. There, they form the characteristic funnel-like structure that is exhibited prominently in Fig. 4d by the magnetic field lines and the plasma β , which is the ratio of gas pressure to magnetic pressure. Although flux tubes are rather rare in this weak field

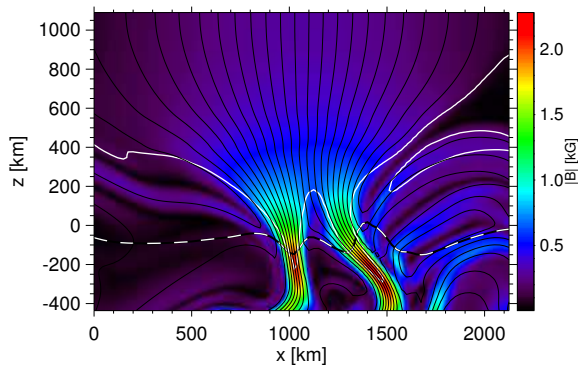


Figure 5. Close-up of a run with higher initial magnetic field strength of $B_0 = 100$ G. Plotted are absolute magnetic field strength (colour), height for optical depth unity (dashed), contour for plasma beta $\beta = 1$ (solid white), and magnetic field lines (solid black).

simulation, they seem to form a “small-scale canopy” that is also present in the 3D model. The average height where plasma $\beta = 1$ exceeds the upper boundary of the model for 47% of all columns (for the whole simulation sequence). The 3D model has a higher extent so that the $\beta = 1$ -surface lies almost everywhere in the computational domain, resulting in a value of 990 km with a standard deviation of 150 km. Apart from flux tubes the field is concentrated in narrow sheets close to the surface of optical depth unity and is strongly reduced in the low and middle photosphere as result of lateral flows above granules that advect the magnetic field towards the intergranular lanes, leaving weak field behind only.

The chromosphere is filled with magnetic field more homogeneously compared to the photosphere below since the flux tube funnels spread out in this thinner regime until they cover the whole horizontal extent. The field is very dynamic due to the propagation of shock waves that – like already in the non-magnetic simulations by Wedemeyer et al. (2004) – are a ubiquitous phenomenon in the model chromosphere. An example can be seen in the upper right corner of the snapshots, best in gas temperature (Fig. 2a) and velocity (Fig. 2d). The shock wave sweeps and densifies the magnetic field, forming a thin filament of enhanced magnetic field (see Fig. 4 close to $x = 4200$ km and $z = 700$ km). The chromosphere is filled with this kind of filament that have a field strength of not more than a few tens of Gauss. The weak field filaments form, move, and eventually dissolve quickly with the traversing shock fronts, giving rise to a highly dynamic chromospheric field that evolves on very short time scales, much shorter than in the photosphere or in the convection zone. It is conceivable that these transient phenomena excite magneto-acoustic waves and Alfvén waves propagating along selected magnetic lines of force.

6. OUTLOOK

The presented models and first results just illustrate the beginning of a large series of enhanced models of the lower solar atmosphere, now including the chromosphere that has been difficult to model so far. The radiation magnetohydrodynamics code CO⁵BOLD is under continuous development. For the future, important points to work on concern the radiative transfer in the chromosphere and its influence on the energy balance of these layers, as well as a transmitting upper boundary condition for the MHD case. Future models will have higher spatial resolution on the one hand and a larger spatial extension in horizontal but also in vertical direction on the other. An important goal is a sequence of simulations with different magnetic field strength that will allow the investigation of the transition and difference of the magnetic network and the weak field cell interiors.

ACKNOWLEDGMENTS

SW was supported by the *Deutsche Forschungsgemeinschaft (DFG)*, project Ste 615/5. WS acknowledges support by the *Austrian Fonds zur Förderung der wissenschaftlichen Forschung (Erwin-Schrödinger-Stipendium)*, project No. J2211.

REFERENCES

- Asensio Ramos, A., Trujillo Bueno, J., Carlsson, M., & Cernicharo, J. 2003, *ApJL*, 588, L61
- Freytag, B., Steffen, M., & Dorch, B. 2002, *Astron. Nachr.*, 323, 213
- Höfner, S., Gautschy-Loidl, R., Aringer, B., et al. 2004, in *ESO Workshop “High Resolution Infrared Spectroscopy in Astronomy”*, eds. Käufel H.U., Siebenmorgen R., Moorwood A., Springer, 11P
- Leenaarts, J. & Wedemeyer-Böhm, S. in prep.
- Schaffenberger, W., Steiner, O., & Wedemeyer-Böhm, S. in these proceedings
- Schüssler, M., Shelyag, S., Berdyugina, S., Vögler, A., & Solanki, S. K. 2003, *ApJL*, 597, L173
- Shelyag, S., Schüssler, M., Solanki, S. K., Berdyugina, S. V., & Vögler, A. 2004, *A&A*, 427, 335
- Steiner, O., Hauschildt, P. H., & Bruls, J. 2001, *A&A*, 372, L13
- Uitenbroek, H. 2000, *ApJ*, 531, 571
- Wedemeyer-Böhm, S., Kamp, I., Bruls, J., & Freytag, B. 2005, *A&A*, 438, 1043
- Wedemeyer-Böhm, S., & Steffen, M. 2005, in prep.
- Wedemeyer, S., Freytag, B., Steffen, M., Ludwig, H.-G., & Holweger, H. 2004, *A&A*, 414, 1121
- Wedemeyer, S. 2003, PhD thesis, University of Kiel, <http://e-diss.uni-kiel.de/diss.764/>